Iraqi Journal of Science

ISSN: 0067-2904

Shell Model Calculations for Some Properties of $^{29-34}$Mg Isotopes

Lubna Abduljabbar Mahmood, Ghaith Naima Flaiyh
Department of Physics, College of Science, Baghdad University, Baghdad, Iraq

Received: 28/9/2020 Accepted: 17/3/2021

Abstract

The calculations of the shell model, based on the large basis, were carried out for studying the nuclear $^{29-34}$Mg structure. Binding energy, single neutron separation energy, neutron shell gap, two neutron separation energy, and reduced transition probability, are explained with the consideration of the contributions of the high-energy configurations beyond the model space of sd-shell. The wave functions for these nuclei are used from the model of the shell with the use of the USDA 2-body effective interaction. The OBDM elements are computed with the use of NuShellX@MSU shell model code that utilizes the formalism of proton-neutron.

Keywords: Shell model, binding energy, single neutron separation energy, neutron shell gap, two neutron separation energy.

حسابات أنموذج القشرة لبعض خصائص نوى نظائر $^{29-34}$Mg

لبنى عبد الجبار محمود*،غيث نعمة فليح
قسم الفيزياء ، كلية العلوم ، جامعة بغداد ،بغداد ، العراق

الخلاصة

تم استخدام حسابات أنموذج القشرة مع الأخذ لمدى واسع من التوزيعات لدراسة التركيب النووي لنظائر المغنيسيوم$^{29-34}$Mg حيث تم تفسير كل من طاقة الربط ،طاقة الفصل للنيوترون، فجوة غلاف النيوترون, طاقة فصل النيوترونين واحتمالية الانتقال الكهربائي المختزلة بالاعتماد على مساهمات التوزيعات ضمن مدى الطاقة العالي لفضاء القشرة –sd.الدوال الموجية لهذه النوى حسبت بالاعتماد على أنموذج القشرة باستخدام التفاعل المؤثر لجسيمتين (USDA–2) لهذه النوى، وتم حساب OBDMباستخدام برنامجNuShellX@MSU على صيغة بروتون – نيوترون .

1- Introduction

There are 22 discovered Mg isotopes. The atomic number of those isotopes is 12 and the neutron number is in the range between 7 and 28. There are 3 stable isotopes, which are ^{24} Mg, ^{25} Mg, and ^{26} Mg, as well as 19 other radio-isotopes. ^{28} Mg can be considered as the longest-lived radio-isotope that has a 20.915h half-life. The radioisotope which is shortest-lived is the rare ^{40} Mg that has an over 170ns half-life [1]. The isotopes which are lighter usually decay to the Na isotopes, whereas the heavy ones decay to the Al isotopes. The isotopic chain of Mg is particularly interesting, due to the unique nuclear structure of those isotopes. That importance is a result of the significance of the nuclei lying far from the ß-stability, as they were proven adequately adapted for descriptions of the nuclear systems which are near the stability valley. Such characteristic made them sufficient testing candidates for the model of the nuclear shell [2]. Those isotopes are the extended chain on both stability valley sides, beyond the shell of N =9, representing neutron deficient side, till the N =17 shell at the rich side of the

*Email: lubna917@yahoo.com

neutron, representing the boundaries of the "inversion islands" [3], which are regions in which the normal shell model theory of the filling of a single-particle level changes due to the overlap in the model spaces [2].

Shell model is a description of the fillings of the shells or the orbits with the specific angular momentum nucleons and spins with augmenting energy in nuclear potential. The shells are filled in such a way which has consistency with the Principle of the Pauli Exclusion, which indicates the fact that every one of the nucleons includes a separate wave function and quantum numbers set. Each one of the nucleons is viewed as a separate particle that orbits in central potential, despite the presence of strong interactions amongst the nucleons [4]. This central potential is responsible for the regulation of the motions of every one of the nucleons, designed for the approximation of the majority of separate interactions of the nucleons [5]

The ground state density values of the proton-rich unstable ^{9}C, ^{12}N & ^{23}Al exotic nuclei was researched through the binary cluster model (BCM) and the two-frequency shell model (TFSM) [6]. In the latter, the wave functions of the single particle harmonic oscillator was utilized with 2 different parameters of the oscillator size $ß_c$ & $ß_v$, where the first is for core (i.e. inner) orbits and the second is for valence (i.e. halo) orbits.

The nuclear structure of the ^{17}O nucleus was investigated using shell model with self-consistent Hartree-Fock calculations [7]. In particular, elastic and inelastic electron scattering form factors, energy levels, and transition probabilities were calculated for positive and negative low-lying states. Two different shell model spaces were used for this purpose. The first one is the *psdpn* model space for positive parity states and the second one is *p1/2sd* model space for negative parity states. For all selected excited states, Skyrme interactions were adopted to generate a one-body potential in Hartrre-Fock theory for calculating the single-particle matrix elements.

The nuclear density distributions, size, radi,i and elastic electron scattering form factors for proton-rich ^{8}B, ^{17}F,^{17}Ne, ^{23}Al, and ^{27}P nuclei were calculated using the radial wave functions of Woods-Saxon potential [8]. The parameters of such potential for nuclei under study were generated so as to reproduce the experimentally available size radii and binding energies of the last nucleons on the Fermi surface.

NuShell-X is a collection of the computer codes that were written by B. Rae [9], which have been utilized for obtaining the accurate values of the energy as well as the Eigen-vectors and the spectroscopic overlap for the low-lying state cases in the shell model Hamilton matrix computations with quite large basis dimension values. It utilizes the J-coupled basis of the proton-neutron and the dimensions of the J-scheme matrix, with an order of about a hundred million that may be taken into consideration. NuShell-X@MSU is a collection of the wrapper codes that were written by A. Brown [10], who used the data files for the model spaces and Hamiltonian for the generation of the input for the NuShell-X.

2- Theory

The reduced element of matrix of electron scattering operators for the n-particle model space wave function of the multi-polarity λ is represented as a summation of products over the elements of the OBDM (i.e. the one-body density matrix) which reduced the elements of the matrix of single-particles, and is represented as [11] :

$$< f \left\| \hat{O}^{\lambda} \right\| i > = < n\omega_f J_f \left\| \hat{O}^{\lambda} \right\| n\omega_i J_i > = \sum_{k_\alpha k_\beta} OBDM\left(fik_\alpha k_\beta \lambda\right) < k_\alpha \left\| \hat{O}^{\lambda} \right\| k_\beta > \quad (1)$$

k represents single-particle states *(n l j)*, *i* & *f* represent, respectively, the initial and the final states of the model space, *(n ω_i J_i)* & *(n ω_f J_f)*. ω represents the variety of the basis states with an identical *J* value. OBDM in the formalism of proton-neutron is represented in the following equation [11],

$$OBDM\left(fik_{\alpha,t_z} k_{\beta,t_z} \lambda\right) = \frac{< n\omega_f J_f \left\| \left[a^{+}_{k_\alpha t_z} \otimes \tilde{a}_{k_\beta t_z} \right]^{\lambda} \right\| n\omega_i J_i >}{\sqrt{2\lambda + 1}} \quad (2)$$

t_z= 1/2 for the neutron and t_z = -1/2 for the proton. For central potentials, Skyrme potential is used, for which the Za2-body interaction is employed. One could generate from it a one-body potential in the theory of the Hartree-Fock, as utilized in codes. It has been expected to be providing the field of the average resulting from all of the nucleons-composing nuclei, and approximating realistic forces of the

nucleon-nucleon (as well as nucleon-nucleon-nucleon). Skyrme potential V_{Skyrme} can be expressed in the following form [12],

$$V_{Skyrme}(\vec{r}_1,\vec{r}_2) = t_0(1+x_0\hat{P}_\sigma)\delta_{12} + \frac{t_1}{2}(1+x_1\hat{P}_\sigma)\left[\vec{k}^2\delta_{12} + \delta_{12}\vec{k}^2\right] + t_2(1+x_2\hat{P}_\sigma)\vec{k}\delta_{12}\vec{k} + \frac{t_3}{6}(1+x_3\hat{P}_\sigma)\rho(\frac{\vec{r}_1+\vec{r}_2}{2})^\alpha\delta_{12} + iW_0\vec{k}\delta_{12}(\hat{\vec{\sigma}}_1+\hat{\vec{\sigma}}_2)\times\vec{k} + \frac{t_e}{6}\left([3(\hat{\vec{\sigma}}_1.\vec{k}')(\hat{\vec{\sigma}}_2.\vec{k}') - (\hat{\vec{\sigma}}_1.\hat{\vec{\sigma}}_2)\vec{k}'^2]\delta_{12} + \delta_{12}[3(\hat{\vec{\sigma}}_1.\vec{k})(\hat{\vec{\sigma}}_2.\vec{k}) - (\hat{\vec{\sigma}}_1.\hat{\vec{\sigma}}_2)\vec{k}^2]\right) + t_0[3(\hat{\vec{\sigma}}_1.\vec{k})\delta_{12}(\hat{\vec{\sigma}}_2.k) - (\hat{\vec{\sigma}}_1.\hat{\vec{\sigma}}_2)\vec{k}'\delta_{12}\vec{k}] \quad (3)$$

$$\delta_{12} = \delta(\vec{r}_1-\vec{r}_2) \quad (4)$$

$$\hat{k} = \frac{1}{2i}(\vec{\nabla}_1-\vec{\nabla}_2),\ \vec{k}' = -\frac{1}{2i}(\vec{\nabla}_1-\vec{\nabla}_2) \quad (5)$$

Those are operators of the relative momentum, operating on the wave function to the right and left. $\hat{P}_\sigma$ represents the operator of the spin-exchange which is represented as:

$$\hat{P}_\sigma = \frac{1}{2}(1+\hat{\vec{\sigma}}_1.\hat{\vec{\sigma}}_2) \quad (6)$$

The terms with the momentum-dependence were provided for taking under consideration the impact of finite-range forces and are significant for the characteristics of the surface [13]. In these computations, two Skyrme parametrization types, SLy-4 [14] and Sk-Xcsb [15], were carried out. Those parameterizations provided a sufficient binding energy reproduction, in addition to RMS radii. In the SLy-4, the correlations of the pairing were included with the use of a density dependent force of 0-range. SkXcsb comprises the CSB (i.e. charge symmetry breaking) in the s-wave part of Skyrme interactions in combination with normal exchange (CE) and CD (i.e. the Coulomb direct) terms. CD potential is resulted from the folding of computed distribution of the charge, $\rho_{ch}(r)$, with a 2-body Coulomb interaction, which is represented by the equation below [16],

$$H_{CD} = \frac{e^2}{2}\int_0^\infty\int_0^\infty\frac{\rho_p(r)\rho_p(r')}{|r-r'|}d^3r\,d^3r' \quad (7)$$

The Coulomb interaction exchanging part is a result of Slater approximations, and it is the 1st density matrix expansion term in local approximation of the density, which is represented by the following equation:

$$H_{CE} = -\frac{3}{4}e^2\left(\frac{3}{\pi}\right)^{1/3}\int_0^\infty\rho_p(r)^{\frac{4}{3}}d^3r \quad (8)$$

Longitudinal (i.e. Coulomb) scattering of the electrons form the factors for the inelastic scattering between the initial (i) and the final (f) states or, for the elastic scatterings (i = f), are represented by the F(Cλ,q,f,i). The transverse magnetic and electric form factors are represented, respectively, as F(Mλ,q,f,i) & F(Eλ,q,f,i), where λ stands for multi-polarity [17]. The last 2 form factor types may be classified to components based upon the currents of convection λ*c* (because of the nucleons orbital motion) and the currents of the magnetization λ*m* (as a result of nucleons inherent magnetic moments) [18], as follows:

$F(E\lambda,q,f,i) = F(E\lambda c,q,f,i) + F(E\lambda m,q,f,i)$(9)

$F(M\lambda,q,f,i) = F(M\lambda c,q,f,i) + F(M\lambda m,q,f,i)$(10)

Therefore, the total longitudinal form factor may be written as:

$|F_C(q,f,i)|^2 = \sum_{\lambda\geq0}|F(C\lambda,q,i,f)|^2$(11)

and the total transverse form factor may be written in the following form:

$|F_T(q,f,i)|^2 = \sum_{\lambda>0}\{|F(E\lambda,q,i,f)|^2 + |F(M\lambda,q,i,f)|^2\}$(12)

The form factors of the electron scattering, which involve the momentum transfer q and the angular momentum λ, between the initial and the final states of the nuclear SM of the spin $J_{i,f}$, are represented as [18]

$$|F(X\lambda,q,f,i)|^2 = N_P \left| \sum_{t_z} \langle n\omega_f J_f \| \hat{O}^{\lambda}(X,q,t_z) \| n\omega_i J_i \rangle|^2 \times F_{cm}^2(q) F_{fs}^2(q) \right| \quad (13)$$

where $N_P = 4\pi/Z^2(2J_i + 1)$ and X chooses the longitudinal (C or L) and the transverse (T) form factors. Some highest importance information of the nuclear physics are included in those two form factors.

$F_{fs}(q)$ represents the finite size (fs) form factor of the nucleon and $F_{cm}(q)$ represents the correction for lack in the translation invariance in SM (i.e. correction of the center-of-mass).

Total form factor represents the summation of transverse and longitudinal terms:

$$|F(q)|^2 = |F_C(q,f,i)|^2 + \left[\frac{1}{2} + tan^2\left(\frac{\theta}{2}\right)\right] |F_T(q,f,i)|^2 \quad (14)$$

θ stands for the angle of the scattering of the electrons. The probability of the decreased transition can be expressed as [11,18]

$$B(X\lambda) = \frac{Z^2}{4\pi}\left[\frac{(2\lambda+1)!!}{k^{\lambda}}\right]^2 |F(X\lambda,k)|^2 \quad (15)$$

where $k = E_x/\hbar c$.

B(M1) is in u_N^2, B(E2) is in e^2fm^4 units, B(M2) is in $u_N^2 fm^2$ units, and B(E1) is in e^2fm^2 units, where u_N represents nuclear magnet on $u_N = \frac{e\hbar}{2m_pC} = 0.1051\ e\ fm$.

2.1. Nuclear Binding Energy

NuShell-X is utilized for obtaining the accurate energy values [9], Eigen-vectors, and spectroscopic overlaps of the low-lying states in Hamilton matrix computations' shell model with quite large dimensions of the basis. It utilizes the basis of the J-coupled proton-neutron and the dimensions of the J-scheme matrix of up to an order of a hundred million that may be taken into consideration.

$$H = H_{pp} + H_{pn} + H_{nn} \quad (16)$$

The 2nd quantized H_{pn} form can be represented as [18]:

$$H_{pn} = \sum_{pn\acute{p}\acute{n},J_o} \left\{[a_p^+ a_n^+]^{J_o} \otimes [\tilde{a}_{\acute{p}} \tilde{a}_{\acute{n}}]^{J_o}\right\}^{(0)} \quad (17)$$

These operators can be recoupled to

$$\left\{[a_p^+ a_n^+]^{J_o} \otimes [\tilde{a}_{\acute{p}} \tilde{a}_{\acute{n}}]^{J_o}\right\}^{(0)} = -\sum_{\lambda} \sqrt{(2\lambda+1)(2J_o+1)}\,(-1)^{j_n + j_{\acute{p}} - \lambda - J_o} \times \begin{Bmatrix} j_p & j_n & J_o \\ j_{\acute{n}} & j_{\acute{p}} & \lambda \end{Bmatrix} \times \left\{[a_p^+ \tilde{a}_{\acute{p}}]^{\lambda} \otimes [a_n^+ \tilde{a}_{\acute{n}}]^{\lambda}\right\}^{(0)} \quad (18)$$

p represents wave function of the single-particle (n_p, ℓ_p, j_p). As a result, H_{pn} can be expressed in the form of the particle-hole [19],

$$H_{pn} = \sum_{p\acute{p}n\acute{n}\lambda} F_{\lambda}(p\acute{p}n\acute{n}) \left\{[a_p^+ \tilde{a}_{\acute{p}}]^{\lambda} \otimes [a_n^+ \tilde{a}_{\acute{n}}]^{\lambda}\right\}^{(0)} \quad (19)$$

where

$$F_{\lambda}(p\acute{p}n\acute{n}) = -\sum_{j_o} \sqrt{(2\lambda+1)(2J_o+1)}\,(-1)^{n+\acute{p}-\lambda-J_o} \begin{Bmatrix} p & n & J_o \\ \acute{n} & \acute{p} & \lambda \end{Bmatrix} \quad (20)$$

The NuShell-X basis states are given in the following form

$$|B,J> = |[(J_P,\alpha_P) \otimes (J_n,\alpha_n)]\,J> \quad (21)$$

For Lanczos multiplications of H_{pp}:

$$\delta_{J_{nf},J_{ni}}\delta_{\alpha_{nf},\alpha_{ni}}\delta_{J_{pf},J_{pi}} < (J_{pf},\alpha_{pf})\big|H_{PP}\big|(J_{pi},\alpha_{pi}) >$$

with a similar expression of H_{pp} , and

$$\sum_{p\acute{p}n\acute{n},\lambda} F_\lambda(p\acute{p}n\acute{n}) \times < B_f,J\big|\{[a_p^+\tilde{a}_{\acute{p}}]^\lambda \otimes [a_p^+\,\tilde{a}_{\acute{n}}]^\lambda\}^{(0)}|B_i,J >$$
$$= \sum_\lambda \Gamma_\lambda \sum_{p\acute{p}n\acute{n}} F_\lambda(p\acute{p}n\acute{n})$$
$$\times RDM\big(p_f,p_i,p,\acute{p},\lambda\big)RDM(n_f,n_i,n,\acute{n},\lambda) \quad (22)$$

where p_f represents the labels (J_{pf},α_{pf})

$$\boldsymbol{\Gamma_\lambda} = \begin{Bmatrix} J_{pf} & J_{pi} & \lambda \\ J_{nf} & J_{ni} & \lambda \\ J & J & 0 \end{Bmatrix} \quad (23)$$

and RDM are matrices of the reduced density (for the protons and neutrons):

$$RDM\big(p_f,p_i,p,\acute{p},\lambda\big) = \langle (J_{pf},\alpha_{pf})\big\|[a_p^+\tilde{a}_{\acute{p}}]^\lambda\big\|(J_{pi},\alpha_{pi})\rangle \quad (24)$$

Successive Lanczos multiplication operations result in the vectors

$$|\omega,J\rangle = \sum_{J_p\alpha_p}\sum_{J_n\alpha_n} A\big(J_p,\alpha_p,J_n,\alpha_n,J\big) \times \big|\big[(J_p,\alpha_p)\otimes(J_n,\alpha_n)\big]\,J\rangle \quad (25)$$

Let H_{pn} be an operateson $|\omega_i,J\rangle$ to give,

$$H_{pn}|\omega_i,J\rangle = H_{pn}\big|\omega_f,J\rangle = \sum_{J_{pf}\alpha_{pf}}\sum_{J_{nf}\alpha_{nf}} \acute{A}(J_{pf},\alpha_{pf},J_{nf},\alpha_{nf},J)\big|[(J_{pf},\alpha_{pf})\otimes(J_{nf},\alpha_{nf})]J\rangle \quad (26)$$

with

$$\acute{A}\big(J_{pf},\alpha_{pf},J_{nf},\alpha_{nf},J\big) = \sum_\lambda \Gamma_\lambda \sum_{p\acute{p}n\acute{n}} F_\lambda(p\acute{p}n\acute{n}) \times \sum_{J_{pi}\alpha_{pi}}\sum_{J_{ni}\alpha_{ni}} RDM\big(p_f,p_i,p,\acute{p},\lambda\big)RDM\big(n_f,n_i,n,\acute{n},\lambda\big) \times A\big(J_{pi},\alpha_{pi},J_{ni},\alpha_{ni},J\big) \quad (27)[19]$$

2-2 Energy of the Separation

The minimal amount of the energy which is required for pulling a nucleon apart from the nucleus provides the energy of the separation. It is how much the remaining of the nucleus mass energy is less than the mass energy of the nucleus, with 1 less nucleon and free nucleon [20]. The emphasis of this study has been made on the Separation Energies of the Neutrons. It is known, by the definition of the single neutron's energy of separation [21], that

$$\mathrm{S_n} = \mathrm{E_B(A,Z)} - \mathrm{E_B(A-1,Z)} \quad (28)$$

In a similar manner, the separation energy of 2 neutrons is represented by:

$$\mathrm{S_{2n}} = \mathrm{E_B(A,Z)} - \mathrm{E_B(A-2,Z)} \quad (29)$$

Equations (28) & (29), which are provided above represent the energy of separation according to the binding energy values of 2 successive atomic nuclei. With the use of these equations, the single neutron was calculated, in addition to the separation energies of the double neutrons for a variety of the Ni-28 transition isotopes [22].

2-3 Paring gap

The main characteristic of the pairing relations is the presence of the gap of energy in the spectrum of the excitation, which manifests itself in 2 separate types of the energetic observables: 1st, a gap exists in quasi-particle spectra of the excitation of the even–even nuclei that does not occur in odd–mass number spectra or the odd–odd nuclei, and 2nd, a shift happens between the interpolating ground–state binding energy curves of the even–even in comparison with the odd–mass nuclei that is referred to as odd–even staggering of the mass. Typically, the 2nd phenomenon was utilized for defining experimental pairing gaps, with the assumption that [23]

$$E_{\text{even-even}}(Z,N) = E_0(Z,N)$$

$$E_{\text{odd Z}}(Z,N) = E_0(Z,N) + \Delta_p(Z,N) \quad (30)$$

$$E_{\text{odd N}}(Z,N) = E_0(Z,N) + \Delta_n(Z,N)$$

In the odd–odd nuclei, there was, in addition, the residual interaction between the unpaired neutron and proton; however, this case will not be taken into consideration in this discussion [24].

3- Results and Discussion

The relationship between the number of nucleons and the binding energy is presented in Figure-1 and Table-1, where the number of nucleons on the x-axis as well as the binding energy on the y axis are measured by MeV. The red circles represent the theoretical results and the black circles represent the experimental data [25]. We note that the experimental data [25] are closer to the theoretical calculations. From Figure-1 and Table-1 we observe the increase in the binding energy with increasing the mass number.

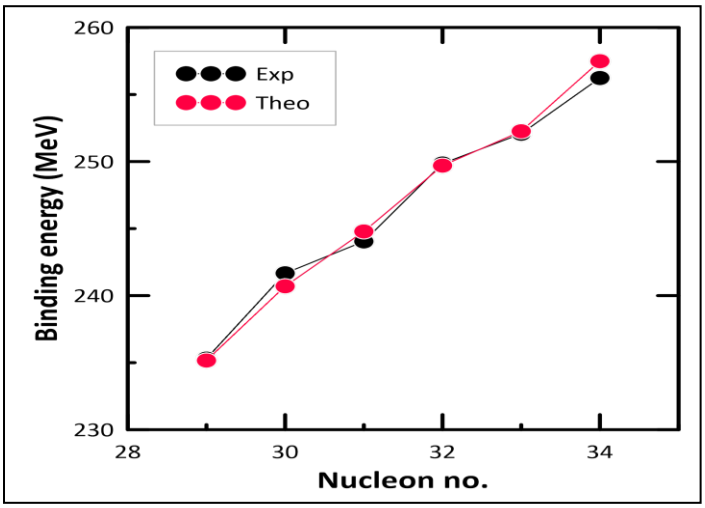

Figure 1- The relation between the number of nucleons for $^{29\text{-}34}$Mg isotopes and the binding energy.

Table 1-The values of binding energy in MeVfor $^{29\text{-}34}$Mg isotopes

Nuclei	Binding energy (MeV) Experiment[25]	Binding energy (MeV) Theory (equ.19)
^{29}Mg	235.303	235.161
^{30}Mg	241.666	240.698
^{31}Mg	244.044	244.786
^{32}Mg	249.854	249.697
^{33}Mg	252.076	252.259
^{34}Mg	256.232	257.486

The relation between one neutron separation energy and the number of nucleons is shown in Figure-2 and Table-2 for $^{29-34}$Mg isotopes. The theoretical results (red circles) approached the experimental data (black circles). It is clear from Figure-2 that the one neutron separation energy for the even nuclei is higher than that of the odd nuclei. This is related to the effect of duplication on the binding energy, where the binding energy for the neutron is larger than that for the nuclei with odd number. From Figure-2 and Table-2, we notice that the separation energy of the neutron is higher in isotopes with even mass number than those with odd ones.

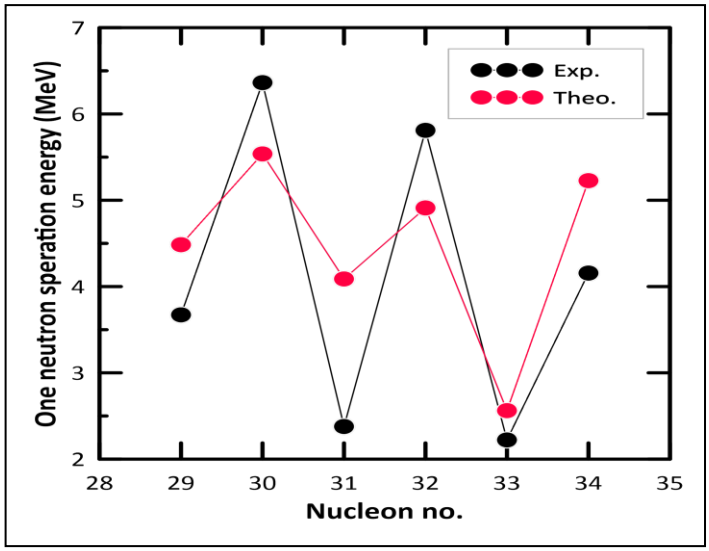

Figure 2- The relation between one neutron separation energy and the number of nucleons.

Table 2-The values of one neutron energy of separation in the MeVfor $^{29-34}$Mg isotopes

Nuclei	One neutron separation energy (MeV), Experimental [25]	One neutron separation energy (MeV), Theoretical
^{29}Mg	3.672	4.485
^{30}Mg	6.363	5.537
^{31}Mg	2.378	4.088
^{32}Mg	5.81	4.911
^{33}Mg	2.222	2.562
^{34}Mg	4.156	5.227

The relation between the energy of the two neutrons separation and the number of nucleons is represented in Figure-3 and Table-3 for $^{29-34}$Mg isotopes. This figure shows the theoretical results and experimental data. It can be observed that the two neutrons separation energy is decreased when the number of nucleons is increased; as the nucleons move away from the center of the nuclei, this means that the binding energy of nucleon is decreased when the number of nucleons is increased.

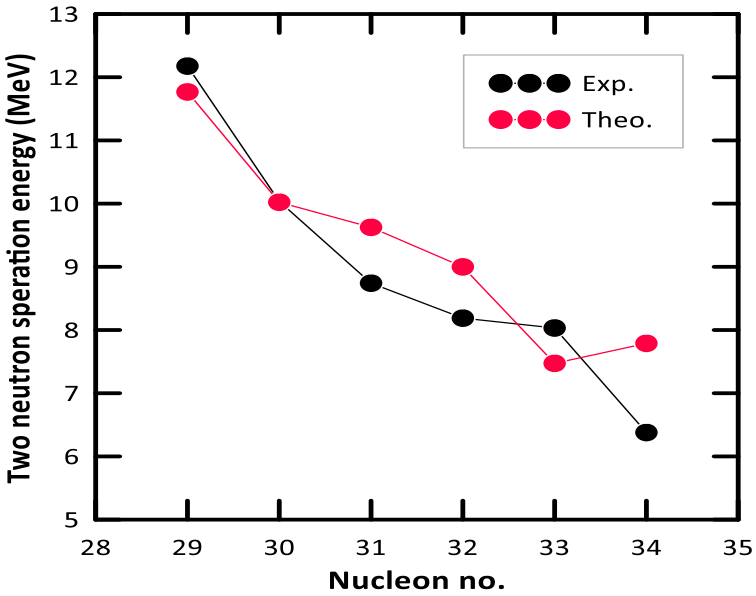

Figure 3- The relation between the two neutrons separation energy and the number of nucleons.

Table 3-Two neutron separation energy (equ.29)

Nuclei	Two neutron separation energy (MeV) Experiment [25]	Two neutron separation energy (MeV) Theory
^{29}Mg	12.176	11.767
^{30}Mg	10.035	10.022
^{31}Mg	8.741	9.625
^{32}Mg	8.188	8.999
^{33}Mg	8.032	7.473
^{34}Mg	6.378	7.789

Figure-4 and Table-4 show the relation between the neutron shell gap and the number of nucleons for $^{29\text{-}34}$Mg. The magnitude of the neutron shell gap for the odd nuclei was observed to be higher than that for the even nuclei. This is due to the fact that the binding energy for the even nuclei is higher than that of the odd nuclei. Finally, it is observed that the experimental data [25] are closer to the theoretical calculations.

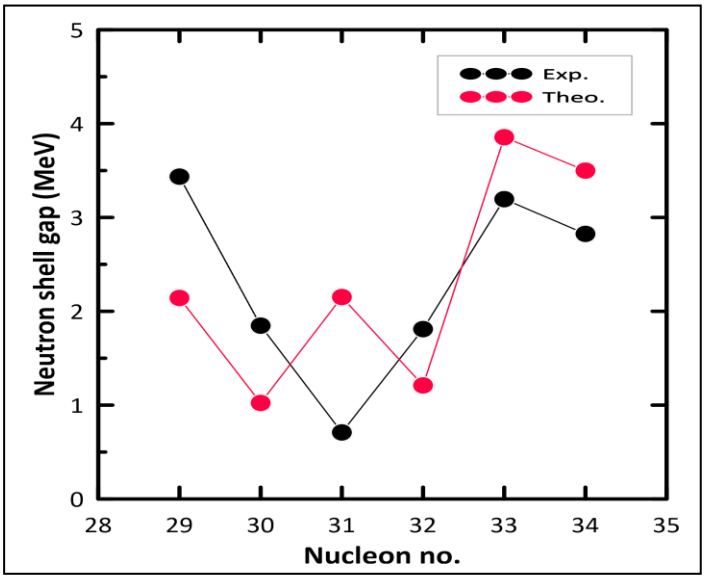

Figure 4- The relation between neutron shell gap and the number of nucleons for $^{29\text{-}34}$Mg isotopes.

Table 4-The values of shell gap in MeV for $^{29-34}$Mg isotopes

Nuclei	Neutron shell gap (MeV) Experiment[25]	Neutron shell gap (MeV) Theory
^{29}Mg	3.435	2.142
^{30}Mg	1.847	1.023
^{31}Mg	0.709	2.152
^{32}Mg	1.81	1.21
^{33}Mg	3.195	3.855
^{34}Mg	2.825	3.499

Figure-5 and Table-5 show the relation between the reduced transition probabilities and the number of nucleons, where the number of nucleons is expressed on the x-axis and the reduced transition probabilities on the y-axis. Red circles represent theoretical values and black circles represent experimental values [26]. Figure-5-a illustrates the systematic behavior of the electromagnetic transition probabilities B(E2) in the Mg isotopes chain. From the comparison between theoretical results and experimental data, we observes large differences. The comparison with the excitation energies is shown in Figure-5-b. In this figure, we observed good agreement between theoretical and experimental results for excitation energy.

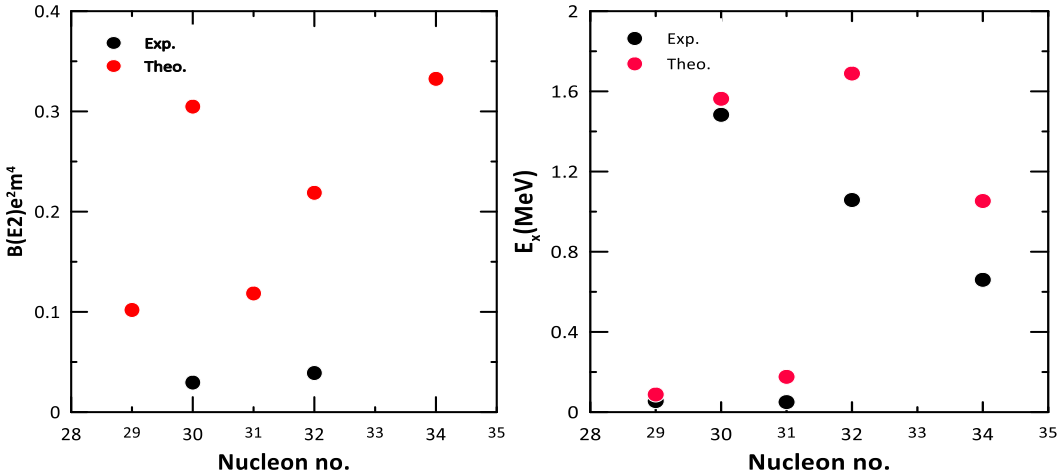

Figure 5-a) The relation between the reduced transition probabilities and the number of nucleon. (b) The relation between the excitation energy and the number of nucleon.

Table (5 a)-The values of reduced transition probabilities

Nuclei	Reduced transition probabilities Theory	Reduced transition probabilities Experiment[26]
^{29}Mg	0.1019	--
^{30}Mg	0.3048	0.0295
^{31}Mg	0.1184	--
^{32}Mg	0.2188	0.039
^{34}Mg	0.3325	--

Table 5-b): The values of excitation energy

Nuclei	Excitation energy theory	Excitation energy experiment
^{29}Mg	0.088	0.055
^{30}Mg	1.563	1.483
^{31}Mg	0.176	0.05
^{32}Mg	1.689	1.058
^{34}Mg	1.053	0.66

Conclusions

Several conclusions could be drawn from the present work; for instance, moving toward neutron-rich nuclei has many effects on the behavior of the isotopes, and the even isotopes give results in a better approach to the process than to the individual. The extrapolation of the binding energies revealed that the nuclei approaching the neutron-rich dripline have relatively higher binding energies than ^{29}Mg. the results also revealed that the one neutron separation energy is decreased when the number of neutron increases and that the neutron separation energy for the even nuclei is higher than that of the odd nuclei for $^{29-34}$Mg isotopes, which occure due to nucleons pairing. Whereas, the two neutrons separation energy is decreased when the number of nucleons is increased for $^{29-34}$Mg isotopes, which gives an indication of unstable nuclei. Additionally, the magnitude of neutron shell gap for the odd nuclei has relatively higher values than that for the even nuclei, due to the fact that the binding energy for the even nuclei is higher than that for the odd nuclei for $^{29-34}$Mg isotopes.

References

1. B.A. Brown, and B.H. Wildenthal, **1988**." Status of the Nuclear Shell Model", *Annu. Rev. Nucl. Part. Sci.* **38**(29): 29-66.
2. A. A.Mohammed. **2015**. "Nuclear Shell Structure of Odd-A Magnesium Isotopes within USDA Hamiltonian", PhD. Thesis, University of Malaya, Kuala Lumpur, Malaysia.
3. J.M. Yao et al. **2011**." Configuration mixing of angular-momentum-projected triaxial relativistic mean-field wave functions. II. Microscopic analysis of low-lying states in magnesium isotopes",*Phys. Rev. C*, **83**: 014308-014409.
4. M.a.J. Mayer, and J. Hans. **1955**. "*Elementary Theory of Nuclear Shell Structure*", New York, John Wiley and Sons, p.1-15.
5. R.F. Casten. **1990**. "*Nuclear Structure from a Simple Perspective*", New York, Oxford University Press, p.3.
6. Adel K. Hamoudi, Gaith N. Flaiyh , Ahmed N. Abdullah. **2015**. "Study of Density Distributions, Elastic Electron Scattering form factors and reaction cross sections of ^{9}C, ^{12}N and 23Al exotic nuclei" *Iraqi Journal of Science*, **56**(1A): 147-161.
7. Ali A. Alzubadi, R. A. Radhi, and Noori S. Manie. **2018**. "Shell model and Hartree-Fock calculations of longitudinal and transverse electroexcitation of positive and negative parity states in ^{17}O *"physical review c*, **97**: 024316-024327.
8. Rafah I. Noori and Arkan R. Ridha; **2019**. " Density Distributions and Elastic Electron Scattering Form Factors of Proton-rich ^{8}B,^{17}F,^{17}Ne,^{23}Al and ^{27}P nuclei" *Iraqi Journal of Science,*
9. NuShellX, W.D.M. Rae, http://www.garsington. eclipse.co.uk.
10. NuShellX@MSU, B.A. Brown, W.D.M. Rae, E. McDon- ald and M. Horoi, http://www.nscl.msu.edu/ resources/resources.html.
11. B. A. Brown, **2005**. "Lecture Notes in Nuclear Structure Physics", *National Superconducting Cyclotron Laboratory and Department of Physics and Astronomy*, Michigan State University, *E. Lansing, MI* 48824.
12. D. Vautherin and D. M. Brink. **1972**. " Hartree-Fock Calculations with Skyrme's Interaction. I. Spherical Nuclei", *Phys. Rev. C*, **5**: 626-647.
13. H. Sagawa, B. A. Brown, and O. Scholten. **1985**." Shell-model calculations with a skyrme-type effective interaction", *Phys. Lett. B*, **159**: 228-232.
14. E. Chabanat, R. Bonche, R. Haensel, J. Meyer, and R. Schaeffer. **1998**. " A Skyrme parametrization from subnuclear to neutron star densities Part II. Nuclei far from stabilities", *Nucl. Phys. A*, **635**: 231-256.
15. B. A. Brown, W. A. Richter, and R. Lindsay. **2000**. " Displacement energies with the Skyrme Hartree–Fock method", *Phys. Lett. B* **, 483**: 49-54.
16. J. W. Negele and D. Vautherin. **1972**." Density-Matrix Expansion for an Effective Nuclear Hamiltonian", *Phys. Rev. C* **, 5**: 1472-1493.
17. T. de Forest and J. D. Walecka. **1966**. " Electron scattering and nuclear structure", *Adv. Phys*., **15**.
18. B. A. Brown, B. H. Wildenthal, C. F. Williamson, F. N. Rad, S.Kowalski, H. Crannell, and J. T. O'Brien. **1985**. " Shell-model analysis of high-resolution data for elastic and inelastic electron scattering on 19F", *Phys. Rev. C* , **32**:1127-1156.

19. E. Caurier, G. Martinez-Pinedo, F. Nowacki, A. Poves, J. Retamosa and A.P. Zuker. **1999**. " Full 0ħω shell model calculation of the binding energies of the $1f_{7/2}$ nuclei" *Phys. Rev. C*, **59**: 2033-2039.
20. Krane, K. S.**1988**. "*Introductory Nuclear Physics*", New Jersey, Wiley.
21. Brink, D. M. **2005**. "*Nuclear Superfluidity: Pairing in Finite Systems*", Cambridge, Cambridge University Press.
22. National Nuclear Data Center, Brookhaven National Laboratory. Based on ENSDF and the Nuclear Wallet Cards. Retrieved, from the website: www.nndc.bnl.gov/chart
23. D. G. Madland, and J. R. Nix.**1988**. *Nucl. Phys*. A476, 1.
24. M. Bender, K. Rutz1, P. Reinhard, and J. A. Maruhn, **2000**. "Pairing Gaps from Nuclear Mean–Field Models",*European Physical Journal* , **8**.
25. National Nuclear Data Center (NNDC), https://www.nndc.bnl.gov/
26. S. Raman, C. W. Nestor, JR., and P. Tikkanen**. 2001**. "Transition probability fromthe Ground tothe first – excited 2C state of even–even nuclides"*Atomic Data and Nuclear Data Tables* , **78**: 1–128.